nature geoscience

ARTICLES

https://doi.org/10.1038/s41561-019-0450-3

Reduced continental weathering and marine calcification linked to late Neogene decline in atmospheric CO_2

Weimin Si[1,2*] and Yair Rosenthal[1,2]

The globally averaged calcite compensation depth has deepened by several hundred metres in the past 15 Myr. This deepening has previously been interpreted to reflect increased alkalinity supply to the ocean driven by enhanced continental weathering due to the Himalayan orogeny during the late Neogene period. Here we examine mass accumulation rates of the main marine calcifying groups and show that global accumulation of pelagic carbonates has decreased from the late Miocene epoch to the late Pleistocene epoch even though $CaCO_3$ preservation has improved, suggesting a decrease in weathering alkalinity input to the ocean, thus opposing expectations from the Himalayan uplift hypothesis. Instead, changes in relative contributions of coccoliths and planktonic foraminifera to the pelagic carbonates in relative shallow sites, where dissolution has not taken its toll, suggest that coccolith production in the euphotic zone decreased concomitantly with the reduction in weathering alkalinity inputs as registered by the decline in pelagic carbonate accumulation. Our work highlights a mechanism whereby, in addition to deep-sea dissolution, changes in marine calcification acted to modulate carbonate compensation in response to reduced weathering linked to the late Neogene cooling and decline in atmospheric partial pressure of carbon dioxide.

Earth's climate in the Neogene (~23–2.58 million years ago (Ma)) was characterized by successive cooling steps that culminated in Quaternary glaciations[1]. The origin of this long-term cooling, however, remains debatable. On geological timescales, the atmospheric partial pressure of carbon dioxide (p_{CO_2}), considered the prime climate forcing, is regulated through the balance between volcanic/metamorphic outgassing, silicate weathering and organic matter burial[2]. In the Neogene, seafloor spreading rates and, by inference, outgassing rates appear to have been relatively constant[3], leading to the corollary that the Neogene decrease in p_{CO_2} and climate cooling may have been primarily driven by enhanced weathering; it has been argued that the Neogene uplift of the Himalayas may have enhanced rock weathering due to increased exposure of weatherable rock surfaces[4,5]. The weathering hypothesis (Raymo's hypothesis), however, is controversial because it argues that weathering can act as a forcing rather than a stabilizing feedback of Earth's thermostat[2,6,7]. The alternative hypothesis (Berner's hypothesis) relates high weathering fluxes to the impact of high atmospheric p_{CO_2} and warm surface temperatures, which provide a necessary feedback to stabilize climate[2]. Accordingly, Neogene cooling should have resulted in reduced, rather than enhanced, continental weathering.

In a steady-state ocean, weathering fluxes of dissolved solutes to the sea must be balanced by output fluxes. With regard to the ocean's carbonate alkalinity budget, the balance between riverine alkalinity input and $CaCO_3$ burial is achieved through $CaCO_3$ dissolution. Pelagic calcifying species, planktonic foraminifera and coccolithophores produce today ~50 Tmol yr^{-1} carbonates in the upper ocean[8–10], consuming approximately three times the alkalinity that is made available to the ocean from rivers (~33 Teq yr^{-1} (ref. [11])). To restore the ocean's alkalinity budget, dissolution will take place in the deep sea. The balancing process is arguably manifested in the calcite compensation depth (CCD)[12], below which seawater is sufficiently undersaturated to dissolve all $CaCO_3$. Raymo's hypothesis[4] and Berner's hypothesis[2] have different predictions as to the change in global $CaCO_3$ burial through the Neogene. Berner's hypothesis predicts high alkalinity and burial fluxes in the early Neogene decreasing to the present, whereas Raymo's hypothesis predicts the opposite. These trends should, in principle, be reflected in the CCD.

For the past 15 Myr, the globally averaged CCD has deepened by ~500 m (ref. [13]). This deepening has been interpreted as increased carbonate burial fluxes in response to higher riverine alkalinity input as the result of enhanced chemical weathering from mountain building[4,5]. However, the CCD-based interpretation relies critically on the assumption of constant carbonate production. Instead, we propose that environmentally driven changes in the production of marine calcifiers have also played an important role in the long-term calcite compensation, thereby modulating the pelagic carbonate burial rate. This supports recent model results suggesting that the CCD alone is insufficient to constrain either the dissolution or the accumulation of pelagic carbonate[14]. Therefore, instead of reconstructing the palaeo-CCD, as was done previously, we reconstruct late Neogene (0–15 Ma) pelagic carbonate production and dissolution by documenting mass accumulation rates of carbonate sediment (MAR_c) and its main producers, coccolithophores ($MAR_{coccolith}$) and planktonic foraminifera (MAR_{foram}), from various ocean basins and depths (Fig. 1), particularly along depth transects where the effects of production and dissolution can be distinguished. Because coccolithophores and foraminifera are different in terms of their ecology (autotrophic versus heterotrophic) and calcification processes, distinguishing between the histories of $MAR_{coccolith}$ and MAR_{foram} is critical to an improved understanding of long-term carbonate cycle changes. Application of this approach to five deep-sea cores selected above the lysocline (<2.6 km depth) suggests that decreasing pelagic carbonate burial rates over the late Neogene were probably driven by decreasing $MAR_{coccolith}$, possibly in response to a decline in continental weathering[15]. Here we extend the study to

[1]Department of Earth and Planetary Sciences, Rutgers University, Piscataway, NJ, USA. [2]Department of Marine and Coastal Sciences, Rutgers University, New Brunswick, NJ, USA. *e-mail: weimin_si@brown.edu

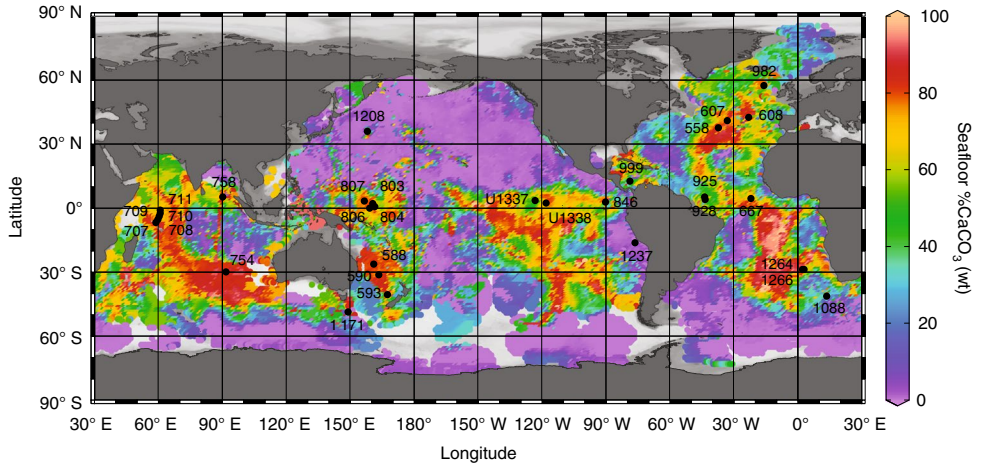

Fig. 1 | Deep-sea sites plotted with gridded seafloor %$CaCO_3$ (ref. [40]). We focus on open ocean sites from mid and low latitudes that are ecologically favoured by pelagic calcifiers and where the seafloor is above the CCD. Pelagic settings that satisfy both criteria account for most pelagic carbonate accumulation[9,40]. The map was prepared using Ocean Data View[41].

more than 30 sites to test the globality of the suggested changes and provide stronger constraints on its causes and implications to the carbon cycle.

Changes in MAR_c over the past 15 Myr

Among the MAR_c records we investigated, many show a decreasing trend following the late Miocene productivity pulse to the late Pleistocene, consistent with previous studies[15,16]. To summarize the trends, we average the MAR_c in three approximately evenly spaced intervals, that is, Pleistocene, 0–2.5 Ma, late Miocene, 5.3–7.5 Ma, and middle Miocene, 11.5–13.5 Ma (Fig. 2 and Supplementary Table 3). Multimillion-year averages are used because they presumably reflect long-term steady states and minimize age model uncertainties. Because a range of processes can affect local carbonate accumulation, temporal variations of MAR_c from the middle–late Miocene to the Pleistocene are expected to be spatially heterogeneous. Two global features, however, stand out.

First, MAR_c have decreased significantly in relatively shallow sites (<3,000 metres below sea level (mbsl)) but show little variation in deeper sites. This is best illustrated by two depth transects in the equatorial Pacific (Fig. 2a,b). In the western equatorial Pacific, MAR_c of the shallowest site (site 806) decreased from >4 g cm^{-2} kyr^{-1} in the Miocene to ~1.7 g cm^{-2} kyr^{-1} in the Pleistocene. Concomitantly, MAR_c in the shallow central equatorial Pacific decreased from ~2–3 g cm^{-2} kyr^{-1} to ~1 g cm^{2} kyr^{-1}. By contrast, MAR_c of both regions show little variation at ~4,000 mbsl, consistent with a previous reconstruction suggesting relatively constant CCD in the Pacific since 15 Ma (ref. [17]). Second, large decreases in MAR_c have also occurred in other regions where today's carbonate production and burial potentials are high (Fig. 2c,d), such as the southwest Pacific and North Atlantic[9]. In the North Atlantic, MAR_c of site 982 (1,134 mbsl) decreased from >5 to ~1.5 g cm^{-2} kyr^{-2}. A similar magnitude of decreases is also seen at site 590 at 1,300 mbsl in the western Pacific.

The temporal pattern of decreasing MAR_c becomes less apparent in the equatorial Atlantic and South Atlantic. At site 925, MAR_c have remained approximately constant, decreasing only by ~1 g cm^{-2} kyr^{-1} in the late Pleistocene (Fig. 3 and Supplementary Fig. 1). In the South Atlantic, MAR_c of site 1264 has a temporal pattern (Supplementary Fig. 1) that is more similar to nearby continental margin site 1085[18], high in the late Miocene but low in the Pleistocene as well as in the middle Miocene. In the deep South Atlantic, MAR_c of sites 928 and 1266 show some increases over time, consistent with previous CCD reconstruction of a deepening towards the Pleistocene. Higher Pleistocene MAR_c at site 1266, however, may be partially due to winnowing and redeposition (Supplementary Information). The equatorial Indian Ocean exhibits the lowest pelagic MAR_c (<1.5 g cm^{-2} kyr^{-1}) and the smallest variations (<0.5 g cm^{-2} kyr^{-1}) of all basins throughout the late Neogene (Supplementary Fig. 1).

Dissolution of deep-sea carbonate during the past 15 Myr

Decreases in MAR_c in the Pacific and the Atlantic can be due to increased dissolution and/or decreased production. We examine the carbonate preservation along a depth transect on the Ontong-Java Plateau in the western equatorial Pacific (sites 806–804) where the deep water likely represents the mean ocean. The $CaCO_3$ content at this transect is ~90% between ~15 and 6 Ma decreasing to ~80% during the past 6 Myr (Fig. 3a). Given relatively constant non-carbonate MAR (~0.2–0.4 g cm^{-2} kyr^{-1}, Supplementary Fig. 1), this decrease may be interpreted as increased dissolution in the past 6 Myr, particularly at deep site 804 (3,800 mbsl).

The preservation of the planktonic foraminifera, however, indicates the opposite. We introduce a coccolith-free size dissolution index (CF-size index: weight ratio of >60 μm/>20 μm) to qualitatively evaluate the preservation of planktonic foraminifera (Supplementary Information). Compared with the conventional dissolution index based on coarse fraction content[19–22], the CF-size index examines only the foraminiferal fraction (>20 μm) by excluding the coccolith fraction (<20 μm) that may potentially bias dissolution estimates due to changes in coccolith productivity. Accordingly, high (low) CF-size index values indicate a high (low) degree of foraminiferal shell preservation. From the depth transect of sites 806–804, the CF-size indices show general increasing trends throughout the past ~14 Myr (Fig. 3b), which, in contrast with the interpretation from the %$CaCO_3$, suggests improved preservation over time. The trend of progressively enhanced foraminiferal preservation is only interrupted at ~10–8 Ma when minimum values indicate that about half of the foraminiferal shells in the oozes are in the form of fine fragments (20–60 μm). These changes in preservation can also be visually recognized under the light microscope, which shows increasing abundance of whole-shell foraminifera over time (Supplementary Fig. 7). The CF-size index can also be affected by other processes, including foraminiferal evolution and burial diagenesis, although these processes do not seem to compromise our main conclusion (Supplementary Information).

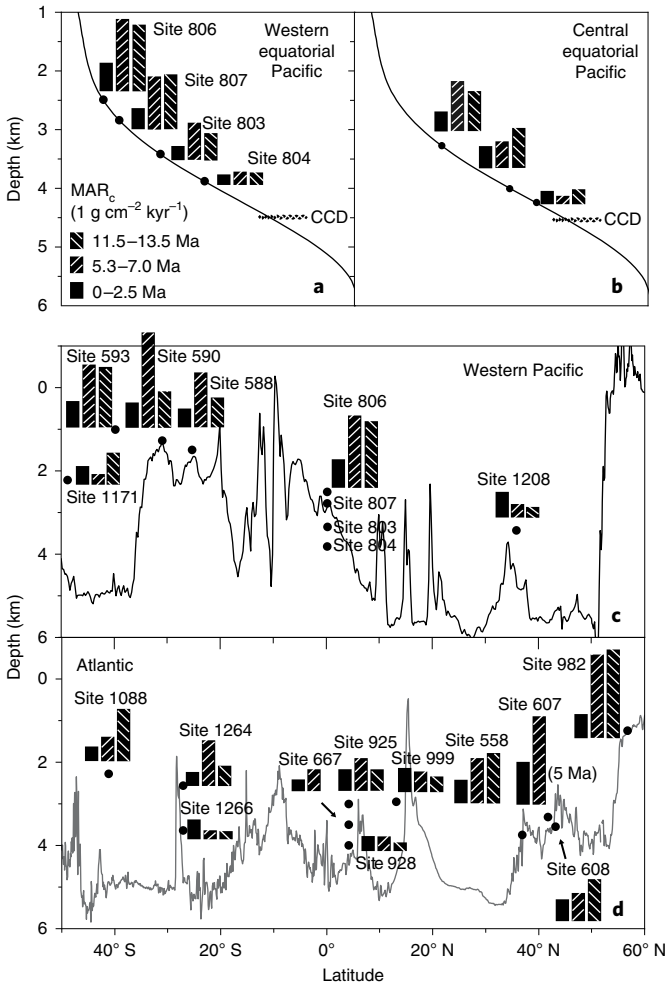

Fig. 2 | Changes in MAR$_c$ in the Pacific and Atlantic oceans. Black lines indicate seafloor bathymetry. **a**,**b**, Equatorial Pacific depth transect. In the central equatorial Pacific, plate movement and ridge subsidence can complicate the temporal trend of MAR$_c$ at a single site due to the large productivity gradient across the region (Supplementary Information). We therefore used a composite MAR$_c$ (Supplementary Fig. 3) to minimize these complications. **c**,**d**, Western Pacific and Atlantic latitudinal transect.

MAR$_{foram}$ from the depth transect further support higher dissolution in the middle–late Miocene. In the Pleistocene, average MAR$_{foram}$ are ~0.45 and ~0.27 g cm^{-2} kyr^{-1} at the shallow site 806 and deeper site 803, respectively, suggesting minimal dissolution between 2,500 and 3,400 mbsl. This estimate is close to Holocene estimates based on radiocarbon ages of core-top materials, which suggest ~0.4 g cm^{-2} kyr^{-1} foraminiferal dissolution over this depth interval (Supplementary Table 5). During 11.5–13.5 Ma, however, the MAR$_{foram}$ were ~1.5 g cm^{-2} kyr^{-1} at site 806 and ~0.25 g cm^{-2} kyr^{-1} at site 803, indicating more than 1 g cm^{-2} kyr^{-1} of planktonic foraminifera had dissolved over the same depth interval.

We also find overall increases in the CF-size index in the southwest Pacific, tropical Indian Ocean, South Atlantic and equatorial Atlantic, even though the timing and patterns vary from site to site (Supplementary Fig. 8). Taken together, our data suggest that the deep sea has become more saturated with respect to carbonate since the middle Miocene.

Linking dissolution to reduced calcification

When carbonate production is constant, the correlation between dissolution and carbonate accumulation is straightforward. More dissolution implies less burial, and vice versa (Supplementary Fig. 9a). Carbonate dissolution can also be affected by the thickness of the transition zone, which is defined as the depth interval between the calcite saturation horizon and the CCD. If the transition zone becomes thicker, dissolution increases even though the CCD remains constant (Supplementary Fig. 9b). Variations in the thickness of the transition zone given constant CCD, therefore, have been invoked to explain changes in carbonate burial[17,23].

Apparently paradoxical evidence of decreasing carbonate accumulation in a progressively more saturated ocean suggests that decreased pelagic carbonate production rather than enhanced dissolution was responsible for reduced carbonate accumulation during the late Neogene. In the modern ocean, sediment traps indicate that the median of carbonate production in mid and low latitudes (60° S–60° N) is ~1.2 g cm^{-2} kyr^{-1} (ref. [24]; Supplementary Fig. 10), a value close to Pleistocene MAR$_c$ of relatively shallow sites where the dissolution effect is limited (Fig. 4). By contrast, MAR$_c$ from the same set of sites suggest much higher carbonate production in the middle–late Miocene.

Because pelagic carbonates are mainly precipitated from coccolithophores and planktonic foraminifera, we calculated MAR$_{foram}$ and MAR$_{coccolith}$ to investigate their relative contributions to higher Miocene MAR$_c$ (Fig. 4 and Supplementary Fig. 1). The calculation shows that MAR$_{foram}$ remained nearly constant over time, whereas MAR$_{coccolith}$ decreased significantly during the late Neogene, consistent with previous findings[15]. As foraminiferal preservation improved during this interval, we conclude that decreasing carbonate production from coccolithophores is responsible for the decreased MAR$_c$.

Changes in carbonate production result in biological compensation[14], complicating the relationships among CCD, carbonate accumulation and saturation state of seawater. For example, although the CCD has remained relatively constant in the equatorial Pacific, dissolution close to the CCD was much stronger in the middle–late Miocene than in the Pleistocene (Fig. 5). However, despite a thicker transition zone and stronger dissolution, carbonate burial within the transition zone was higher in the middle–late Miocene. Overall, it appears that enhanced coccolith production in the Miocene 'outcompeted' stronger dissolution at that time and resulted in higher net carbonate accumulation above the CCD.

Link between marine calcification and weathering

In a steady-state ocean, continental weathering, which is the source of alkalinity in the ocean, is largely balanced by $CaCO_3$ burial. To evaluate the significance of the observed decrease in MAR$_c$ in terms of the ocean carbonate budget, the compensation effects due to a deeper Pleistocene CCD should also be considered. In the North Atlantic, the CCD has likely deepened from ~4 km to ~5 km from the Miocene to the Pleistocene, introducing a compensation effect on the order of ~1.2 g cm^{-2} kyr^{-1} (based on MAR$_c$ estimates for a modern ocean[9], Supplementary Fig. 10). Observed decreases in MAR$_c$, however, vary from ~1 to 4 g cm^{-2} kyr^{-1}. Thus, deeper Pleistocene CCD should have only partially compensated for decreased MAR$_c$. In the equatorial Pacific, carbonate burial has most likely experienced a net decrease given its relatively constant CCD since 15 Ma (ref. [17]). A recent study suggests that CCD might have deepened by ~500 m in this region[25]. However, this deepening only introduces a small burial flux of <0.5 g cm^{-2} kyr^{-1} below 4 km based on a modelling study[9] (Supplementary Fig. 10), which is negligible relative to the reduced carbonate production in our records (2~3 g cm^{-2} kyr^{-1}). Considering the hypsometry of the ocean, we argue that Pleistocene compensation was insufficient to account for the observed large decreases in MAR$_c$ from within and above the transition zone.

In addition to mid- and low-latitude pelagic oceans, MAR$_c$ have also decreased in subpolar regions where coccolith oozes were replaced by diatom oozes in Pleistocene/Pliocene sediments (for example, Ocean Drilling Program (ODP) 747, Kerguelen

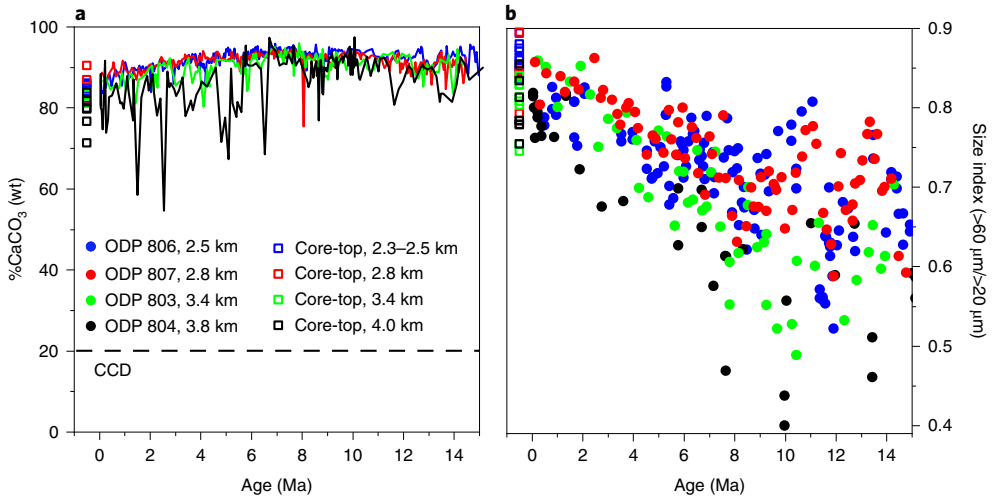

Fig. 3 | Improved preservation of foraminifera in the western equatorial Pacific. a, Bulk %$CaCO_3$ from western Equatorial Pacific. **b**, CF-size index indicates improved preservation of planktonic foraminifers in the past 15 Myr.

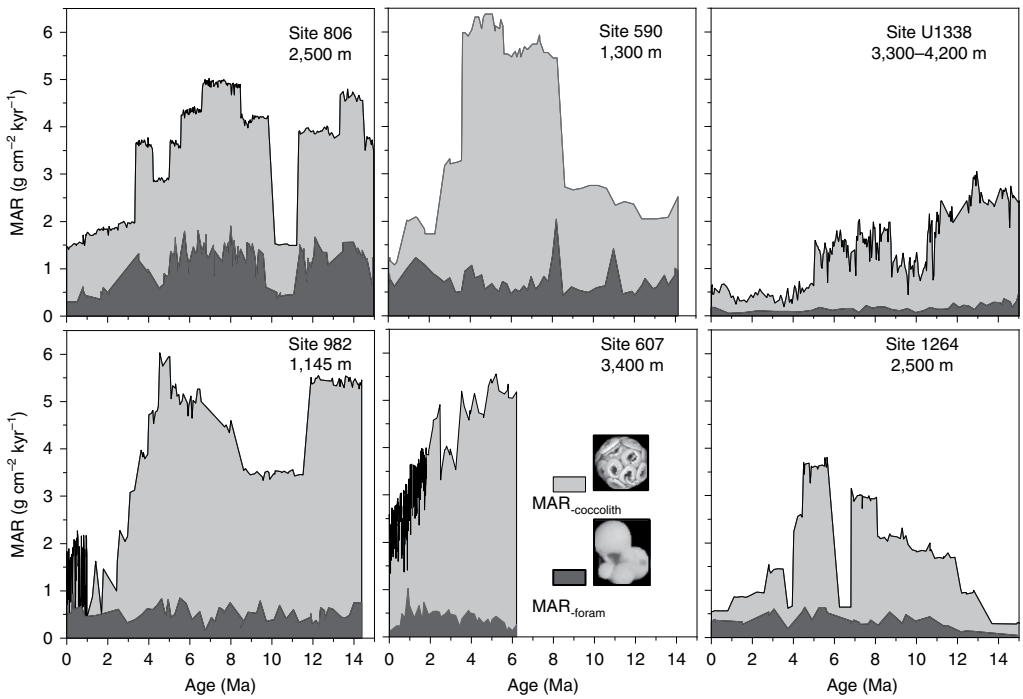

Fig. 4 | Changes in MAR_c, $MAR_{\text{-foram}}$ and $MAR_{\text{-coccolith}}$. Data are presented from six relatively shallow sites where dissolution is not significant.

Plateau[26]). On continental shelves and slopes, carbonate accumulation is also believed to be higher in the Miocene due to higher sea levels[27]. Taking these together, we suggest that global carbonate burial has decreased since 15 Ma, implying that weathering alkalinity input to the ocean has also decreased as the climate has cooled. Although on the basis of our MAR_c records we cannot determine whether the decrease in alkalinity flux represents a change in continental limestone or silicate rock weathering, we note that studies of Himalayas rivers show that carbonate and silicate rocks weathering are potentially coupled[28], leading us to argue that qualitatively, the late Neogene decrease in MAR_c suggests a decrease in the global chemical weathering flux of both rock types in contradiction to the uplift weathering hypothesis[4].

Our argument is further supported by both regional and global proxies indicating changes in chemical weathering. In the South China Sea and the Indian Ocean, chemical and mineralogical indices that have been used to monitor the intensity of chemical weathering suggest a wet climate and strong chemical weathering in the Himalayas during the middle Miocene, followed by a long, steady decline in wetness and weathering after ~10 Ma (ref. [29]). Globally, seawater lithium isotopic ratios (δ^7Li) began to increase at ~15 Ma (ref. [30]). This increase has been interpreted as increasingly incongruent weathering that is characteristic of weathering-limited regimes. Under weathering-limited regimes, weatherable materials such as fresh rocks are in sufficient supply but weathering rates are limited by climatic factors such as temperature and precipitation[31].

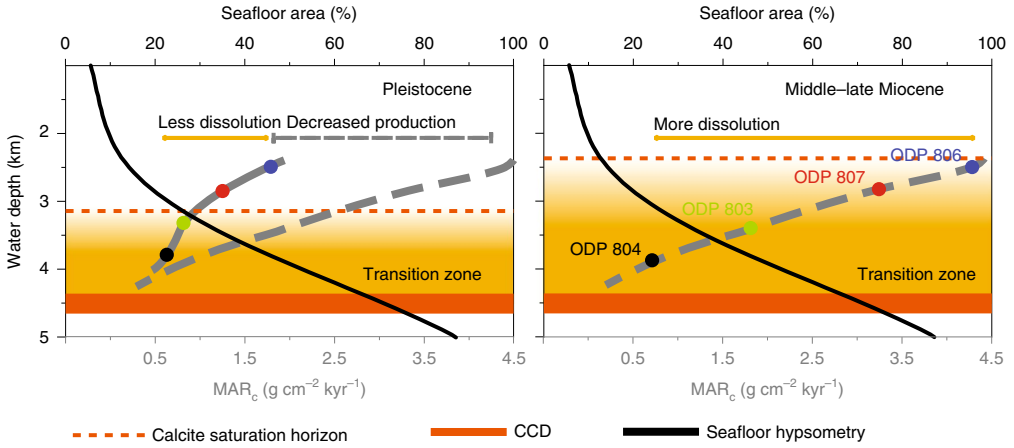

Fig. 5 | Proposed conceptual model for changes in carbonate production, dissolution and accumulation in the late Neogene. The model is compared with depth transect (sites 806–804) in the western equatorial Pacific where deep water is probably representative of the global mean. The Miocene carbonate saturation horizon is estimated on the basis of the large decreases in MAR_c between sites 806 and 807, which suggest that significant dissolution occurred above 2.8 km. Also note that dissolution occurs above the modern calcite saturation horizon in the Pleistocene. Planktonic foraminiferal fauna analysis of core-top materials (Supplementary Fig. 6a)[42] suggests that this is probably due to the dissolution of soluble planktonic foraminifera species. The CCD is placed at ~4.5 km for the past 15 Myr following an earlier study[17].

Increasingly cooling climate in the late Neogene thus should have decreased chemical rock weathering, reducing the alkalinity input to the ocean. Collectively, these records support our interpretation of decreased chemical weathering in a cooling climate.

Essential to our model is a link between biologic[14] and chemical compensation due to concomitant decreases in weathering fluxes and coccolith production over the course of the late Neogene. In other words, the ratio of calcite production to ingredient supply has not undergone large changes through time[32]. This covariation ultimately resulted in relative stability of the CCD. The puzzle is how oligotrophic calcifiers, coccolithophores, are able to 'sense' the changes in continental weathering and 'adjust' their carbonate production accordingly. One hypothesis is that this potential coupling may have occurred through atmospheric p_{CO_2} (refs. [15,33]). In the late Neogene, decreasing p_{CO_2} may have become a limiting factor for photosynthesis in coccolithophores and promoted an active acquisition of cellular CO_2 through carbon concentration mechanisms[34]. Because coccolithophores calcify within the cell, their calcification and photosynthesis machineries probably share the same cellular carbon pool. Hence, carbon concentration mechanisms may have reduced coccolith production through the preferential allocation of cellular carbon uptake for photosynthesis over calcification[34,35] under low p_{CO_2}. Carbon limitation may also favour smaller coccolithophores that have higher surface/volume ratios and may have contributed to the downsizing of coccoliths[15] that is associated with the major taxonomic turnover in the Pliocene[36]. If this is the case, late Neogene $MAR_{coccolith}$ would serve as a good example of how cellular-level evolution has propagated into global effects on geologic timescales.

However, weakened calcification and size reduction could not be the sole driver of a weakened carbonate pump. Changes in nutrient supply probably contributed to regional differences. For example, the persistently low late Neogene carbonate productivity in the equatorial Indian Ocean is probably associated with the absence of major upwelling in the region, whereas higher $MAR_{coccolith}$ in the eastern equatorial Pacific during the middle Miocene may be related to the higher nutrient supplies at that time[37,38]. These observations suggest that changes in coccolith accumulation are probably productivity related. If this is the case, decreasing p_{CO_2} may have affected the coccolith production more indirectly through oceanographic links.

Although specific mechanisms remain to be investigated, we find no evidence for negative feedback between biologic calcification and a more acidic, warmer ocean that is often concerned in the study of future climate changes[39]. Instead, there is apparently much more calcification in the warmer and more acidic Miocene ocean. In the late Neogene, the co-evolution of coccolithophores and continental weathering have resulted in simultaneous decreases in the carbonate production in the surface ocean and the accumulation in the deep sea. As a result, the ocean has become less 'chalky' in both the sunlit zone and the abyss as the Earth has descended into an ice-house world.

Online content

Any methods, additional references, Nature Research reporting summaries, source data, statements of code and data availability and associated accession codes are available at https://doi.org/10.1038/s41561-019-0450-3.

Received: 14 November 2018; Accepted: 15 August 2019;
Published online: 23 September 2019

References

1. Zachos, J., Pagani, M., Sloan, L., Thomas, E. & Billups, K. Trends, rhythms, and aberrations in global climate 65 Ma to present. *Science* **292**, 686–693 (2001).
2. Berner, R. A., Lasaga, A. C. & Garrels, R. M. The carbonate–silicate geochemical cycle and its effect on atmospheric carbon dioxide over the past 100 million years. *Am. J. Sci.* **283**, 641–683 (1983).
3. Rowley, D. B. Rate of plate creation and destruction: 180 Ma to present. *Geol. Soc. Am. Bull.* **114**, 927–933 (2002).
4. Raymo, M. E., Ruddiman, W. F. & Froelich, P. N. Influence of late Cenozoic mountain building on ocean geochemical cycles. *Geology* **16**, 649–653 (1988).
5. Raymo, M. E. Geochemical evidence supporting TC Chamberlin's theory of glaciation. *Geology* **19**, 344–347 (1991).
6. Berner, R. A. & Caldeira, K. The need for mass balance and feedback in the geochemical carbon cycle. *Geology* **25**, 955–956 (1997).
7. Walker, J. C., Hays, P. & Kasting, J. F. A negative feedback mechanism for the long-term stabilization of Earth's surface temperature. *J. Geophys. Res.* **86**, 9776–9782 (1981).
8. Berelson, W. M. et al. Relating estimates of $CaCO_3$ production, export, and dissolution in the water column to measurements of $CaCO_3$ rain into sediment traps and dissolution on the sea floor: a revised global carbonate budget. *Glob. Biogeochem. Cycles* **21**, GB1024 (2007).
9. Dunne, J. P., Hales, B. & Toggweiler, J. R. Global calcite cycling constrained by sediment preservation controls. *Glob. Biogeochem. Cycles* **26**, GB3023 (2012).

10. Milliman, J. D. Production and accumulation of calcium carbonate in the ocean: budget of a nonsteady state. *Glob. Biogeochem. Cycles* **7**, 927–957 (1993).
11. Cai, W. et al. A comparative overview of weathering intensity and HCO_3-flux in the world's major rivers with emphasis on the Changjiang, Huanghe, Zhujiang (Pearl) and Mississippi rivers. *Cont. Shelf Res.* **28**, 1538–1549 (2008).
12. Broecker, W. S. A kinetic model for the chemical composition of sea water. *Quat. Res.* **1**, 188–207 (1971).
13. Van Andel, T. H. Mesozoic/Cenozoic calcite compensation depth and the global distribution of calcareous sediments. *Earth Planet. Sci. Lett.* **26**, 187–194 (1975).
14. Boudreau, B. P., Middelburg, J. J. & Luo, Y. The role of calcification in carbonate compensation. *Nat. Geosci.* **11**, 894–900 (2018).
15. Suchéras-Marx, B. & Henderiks, J. Downsizing the pelagic carbonate factory: impacts of calcareous nannoplankton evolution on carbonate burial over the past 17 million years. *Glob. Planet. Change* **123**, 97–109 (2014).
16. Lyle, M. Neogene carbonate burial in the Pacific Ocean. *Paleoceanography* **18**, 1059 (2003).
17. Pälike, H. et al. A Cenozoic record of the equatorial Pacific carbonate compensation depth. *Nature* **488**, 609–614 (2012).
18. Diester-Haass, L., Meyers, P. A. & Bickert, T. Carbonate crash and biogenic bloom in the late Miocene: evidence from ODP sites 1085, 1086, and 1087 in the Cape Basin, southeast Atlantic Ocean. *Paleoceanography* **19**, PA1007 (2004).
19. Haug, G. H. & Tiedemann, R. Effect of the formation of the Isthmus of Panama on Atlantic Ocean thermohaline circulation. *Nature* **393**, 673–676 (1998).
20. Broecker, W. S. & Clark, E. $CaCO_3$ size distribution: a paleocarbonate ion proxy? *Paleoceanography* **14**, 596–604 (1999).
21. Chiu, T. C. & Broecker, W. S. Toward better paleocarbonate ion reconstructions: new insights regarding the $CaCO_3$ size index. *Paleoceanography* **23**, PA2216 (2008).
22. Bassinot, F. C. et al. Coarse fraction fluctuations in pelagic carbonate sediments from the tropical Indian Ocean: a 1500-kyr record of carbonate dissolution. *Paleoceanogr. Paleoclimatol.* **9**, 579–600 (1994).
23. Farrell, J. W. & Prell, W. L. Pacific $CaCO_3$ preservation and $\delta^{18}O$ since 4 Ma: paleoceanic and paleoclimatic implications. *Paleoceanography* **6**, 485–498 (1991).
24. Honjo, S., Manganini, S. J., Krishfield, R. A. & Francois, R. Particulate organic carbon fluxes to the ocean interior and factors controlling the biological pump: a synthesis of global sediment trap programs since 1983. *Prog. Oceanogr.* **76**, 217–285 (2008).
25. Campbell, S. M., Moucha, R., Derry, L. A. & Raymo, M. E. Effects of dynamic topography on the Cenozoic carbonate compensation depth. *Geochem. Geophys. Geosyst.* **19**, 1025–1034 (2018).
26. Shipboard Scientific Party. Site 747. In *Proc. ODP, Init. Repts* vol. 120 (eds Schlich, R. et al.) 89–156 (Ocean Drilling Program, 1989).
27. Holland, H. D. Sea level, sediments and the composition of seawater. *Am. J. Sci.* **305**, 220–239 (2005).
28. Tipper, E. T. et al. The short term climatic sensitivity of carbonate and silicate weathering fluxes: insight from seasonal variations in river chemistry. *Geochim. Cosmochim. Acta* **70**, 2737–2754 (2006).
29. Clift, P. D. et al. Correlation of Himalayan exhumation rates and Asian monsoon intensity. *Nat. Geosci.* **1**, 875–880 (2008).
30. Misra, S. & Froelich, P. N. Lithium isotope history of Cenozoic seawater: changes in silicate weathering and reverse weathering. *Science* **335**, 818–823 (2012).
31. Kump, L. R. & Arthur, M. A. in *Tectonic Uplift and Climate Change* (ed. Ruddiman, W. F.) Ch. 18 (Plenum Press, 1997).
32. Broecker, W. S. A need to improve reconstructions of the fluctuations in the calcite compensation depth over the course of the Cenozoic. *Paleoceanography* **23**, PA1204 (2008).
33. Hannisdal, B., Henderiks, J. & Liow, L. H. Long-term evolutionary and ecological responses of calcifying phytoplankton to changes in atmospheric CO_2. *Glob. Change Biol.* **18**, 3504–3516 (2012).
34. Bolton, C. T. & Stoll, H. M. Late Miocene threshold response of marine algae to carbon dioxide limitation. *Nature* **500**, 558–562 (2013).
35. Bolton, C. T. et al. Decrease in coccolithophore calcification and CO_2 since the middle Miocene. *Nat. Commun.* **7**, 10284 (2016).
36. Aubry, M.-P. in *Large Ecosystem Perturbations: Causes and Consequences* (eds Monechi S. et al.) 25–51 (Geological Society of America, 2007).
37. Zhang, Y. G., Pagani, M., Henderiks, J., Ren, H. J. E. & Letters, P. S. A long history of equatorial deep-water upwelling in the Pacific Ocean. *Earth Planet. Sci. Lett.* **467**, 1–9 (2017).
38. Lyle, M. & Baldauf, J. Biogenic sediment regimes in the Neogene equatorial Pacific, IODP site U1338: burial, production, and diatom community. *Palaeogeogr. Palaeoclimatol. Palaeoecol.* **433**, 106–128 (2015).
39. Boyd, P. W. Beyond ocean acidification. *Nat. Geosci.* **4**, 273–274 (2011).
40. Archer, D. E. An atlas of the distribution of calcium carbonate in sediments of the deep sea. *Glob. Biogeochem. Cycles* **10**, 159–174 (1996).
41. Schlitzer, R. Ocean Data View v5.1.0 (2018); https://odv.awi.de
42. Berger, W. H., Bonneau, M. C. & Parker, F. L. Foraminifera on the deep-sea floor: lysocline and dissolution rate. *Oceanol. Acta* **5**, 249–258 (1982).

Acknowledgements

We thank M.-P. Aubry for discussion on coccolithophorid taxonomy and evolution, D. Bord for help with nanno-biostratigraphy and the age model, R. Toggweiler for carbonate burial in modern oceans, and X. Zhou for ICP-OES analysis. This work has been partially supported by NSF-OCE grant 634573 to Y.R.

Author contributions

W.S. and Y.R. conceived the idea of a global synthesis of late Neogene mass accumulation rate on pelagic carbonate, foraminifera and coccoliths. W.S. performed the experiments and produced the figures. Both authors contributed to the writing of the manuscript.

Competing interests

The authors declare no competing interests.

Additional information

Supplementary information is available for this paper at https://doi.org/10.1038/s41561-019-0450-3.

Correspondence and requests for materials should be addressed to W.S.

Peer review information Primary Handling Editor(s): James Super; Rebecca Neely.

Reprints and permissions information is available at www.nature.com/reprints.

Publisher's note Springer Nature remains neutral with regard to jurisdictional claims in published maps and institutional affiliations.

Methods

Age model. The age model is based primarily on biostratigraphy in combination with other available data including palaeomagnetic and isotopic records for the Pleistocene and isotope stratigraphy for the middle Miocene intervals. All data are from published work, and a list of references consulted for this work is given in Table S2 of the Supplementary Information. When building an age–depth model, various smoothing methods (that is, the midpoints of the age intervals, spline functions, and so on) are often used to avoid abrupt changes in sedimentation rates with more continuous age–depth function, for example[16]. For this work, we have preferred the step plot because it illustrates clearly the selected age resolution that is considered reasonable and conservative. Given the age–depth models, sample ages were interpolated linearly between two age control points. To build an age model that is robust across geographic locations and water depths (due to dissolution of microfossils), we exclude foraminifera stratigraphy and use nannofossil records only. Not all available biostratigraphic data in the literature are used in our study. To avoid potential complication from inconsistent taxonomy and species identification, we selected only species that are used to define major biozones, which are more reliable and consistently observed. A list of species, depths in each core and ages is available in Supplementary Table 1. The age model is calibrated to the Geologic Time Scale 2012[43].

Mass accumulation rates of carbonates, foraminifera and coccolithophores. Mass accumulation rates of bulk samples (MAR_{bulk}) and MAR_c were calculated using (1) linear sedimentation rates (LSRs) derived from age–depth models, (2) dry bulk density calculated from shipboard moisture and density analyses and (3) carbonate weight percentage (%$CaCO_3$ wt). Specifically, MAR_{bulk} = linear sedimentation rate (cm kyr^{-1}) × dry bulk density (g cm^{-3}), and $MAR_c = MAR_{bulk} \times CaCO_3$ (wt%).

Dry bulk density was calculated from porosity and wet bulk density data based on the following relationship: dry bulk density = wet bulk density − porosity × 1.025. Calculated dry density data were then averaged over 0.5 Myr intervals. Although bulk density data were collected at high resolution in many downcore records, we have used calculated mean values because LSRs can only be calculated at a much lower resolution. Multiplying low-resolution LSRs with high-resolution bulk density data may give a false impression that the MAR variations are known at a high resolution when, in fact, LSR variations on the first order determine the trends.

In addition to %$CaCO_3$ data from the ODP initial report, 500 data points were estimated from calcium measurements of bulk samples using inductively coupled plasma optical emission spectrometry (ICP-OES) at the Department of Marine and Coastal Sciences, Rutgers University. Bulk samples were oven dried and ground into fine powder. About 0.5–0.8 mg powder was then weighed with an accuracy of 0.01 mg before being dissolved in 300 ml of 0.5% acetic acid over 12 h. After centrifugation (10 min at 10,000 rpm), 100 ml of solution was further diluted with HNO_3 to 400 ml for calcium analysis on ICP-OES. Scandium was used as the internal standard for calibration. Calculated calcium was then converted into %$CaCO_3$ of the bulk sample.

To calculate MAR_{foram}, bulk samples were mounted on a McCave rotating carousel for disaggregation for 6–8 h. Previous studies have shown its efficiency in separating coccolith aggregates[34]. The coccolith fraction was then removed through a 20 μm sieve mounted on the vacuum chamber. In the <20 μm fraction, coccoliths were dominant, with only a very minor fraction of planktonic foraminiferal fragments[21]. Independent research that has estimated the contribution of foraminiferal tests from >63 μm and the contribution of coccolith carbonate based on abundance counting and mass conversion[44] also suggest that fine foraminiferal fragments (<63 μm) do not contribute significantly to the bulk carbonate. The >20 μm fraction, however, captures foraminifera and some other minor components (diatoms and radiolarians). MAR_{foram} was then calculated by multiplying weight percentage of foraminifera (>20 μm) with MAR_{bulk}:

$$MAR_{\_foram} = MAR\_bulk \times foraminifera(wt\%)$$
$$\text{Correspondingly, } MAR_{\_coccolith} = MAR_c - MAR_{\_foram}$$

MAR_{bulk}, MAR_c and MAR_{foram} are summarized in Supplementary Fig. 1. All data are available in Supplementary Table 2.

Data availability

The data that support the findings of this study are available within the supplementary information files.

References

43. Gradstein, F. M., Ogg, J. G., Schmitz, M. & Ogg, G. (eds) *The Geologic Time Scale 2012* (Elsevier, 2012)..
44. Baumann, K.-H., Böckel, B. & Frenz M. in *Coccolithophores: From Molecular Processes to Global Impact* (eds Thierstein, H. R. & Young, J. R.) 367–402(Springer-Verlag, 2004).